Flow (2025), **5** E16
doi:10.1017/flo.2025.14

FLOW CAMBRIDGE UNIVERSITY PRESS

RESEARCH ARTICLE

Disentangling coexisting sensory pathways of interaction in schooling fish

Rishita Das[1,2], Sean D. Peterson[3] and Maurizio Porfiri[2,4,5]

[1]Department of Aerospace Engineering, Indian Institute of Science, Bengaluru, KA, India
[2]Department of Mechanical and Aerospace Engineering, New York University Tandon School of Engineering, Brooklyn, NY, USA
[3]Department of Mechanical and Mechatronics Engineering, University of Waterloo, Waterloo, ON, Canada
[4]Center for Urban Science and Progress, New York University Tandon School of Engineering, Brooklyn, NY, USA
[5]Department of Biomedical Engineering, New York University Tandon School of Engineering, Brooklyn, NY, USA
Corresponding author: Maurizio Porfiri; Email: mporfiri@nyu.edu

Received: 21 September 2024; **Revised:** 3 March 2025; **Accepted:** 29 March 2025

Keywords: fish schooling; fluid-structure interaction; information theory; multimodal interactions; time-series analysis

Abstract

Fish swimming together in schools interact via multiple sensory pathways, including vision, acoustics and hydrodynamics, to coordinate their movements. Disentangling the specific role of each sensory pathway is an open and important question. Here, we propose an information-theoretic approach to dissect interactions between swimming fish based on their movement and the flow velocity at selected measurement points in the environment. We test the approach in a controlled mechanical system constituted by an actively pitching airfoil and a compliant flag that simulates the behaviour of two fish swimming in line. The system consists of two distinct types of interactions – hydrodynamic and electromechanical. By using transfer entropy of the measured time series, we unveil a strong causal influence of the airfoil pitching on the flag undulation with an accurate estimate of the time delay between the two. By conditioning the computation on the flow-speed information, recorded by laser Doppler velocimetry, we discover a significant reduction in transfer entropy, correctly implying the presence of a hydrodynamic pathway of interaction. Similarly, the electromechanical pathway of interaction is identified accurately when present. The study supports the potential use of information-theoretic methods to decipher the existence of different pathways of interaction between schooling fish.

Impact Statement

Fish schooling has attracted the interest of the scientific community for centuries. Each school member interacts with others via hydrodynamic, visual and pressure-based pathways, among others, appraising its surroundings and coordinating with others. While we are able to study their coordination by correlating their response to each other's movements, we do not fully understand the contribution of each individual pathway to the collective response. This limits our ability to assess the evolutionary basis and resilience/fragility of collective behaviour and design bio-inspired engineering collectives. In this work, we attempt to segregate the different pathways of interaction simply using measurement data from experimentation in a mechanical system representing two inline-swimming fish. Applying information-theoretic methods, we not only identify a causal dependence between the two fish surrogates but also detect distinct modes of interaction between them. Our data-driven methodology can be applied to several experimental/simulated bio-mechanical complex systems to decipher intermingled pathways of interaction between their units.

1. Introduction

Fish schooling is commonly observed in several species and habitats (Pavlov *et al.* 2000; Filella *et al.* 2018; Pitcher, 2001). Fish coordinate their swimming in terms of distance and speed, maintaining different spatial formations (Ashraf *et al.* 2017; De Bie *et al.* 2020; Saadat *et al.* 2021; Weihs, 1973). Schooling may offer an overall reduced cost of swimming to the entire group (Ashraf *et al.* 2017; Liao *et al.* 2003; Marras *et al.* 2015) and provide advantages in searching for food or route, mating and defending oneself against predators (Landeau & Terborgh, 1986; Larsson, 2012; Major, 1978; Pitcher *et al.* 1982). When swimming in schools, fish interact via different sensory pathways, including hydrodynamic, visual and acoustic, as illustrated schematically in Figure 1a for a fish pair (Weihs, 1973; Ladich & Winkler, 2017; Arnold, 1969; Hyacinthe *et al.* 2019; Kasumyan, 2004; Li *et al.* 2020; Lombana and Porfiri, 2022; Saadat *et al.* 2021; Thandiackal & Lauder, 2023). Fish schooling is the result of complex integration of information from an array of sensory pathways. However, disentangling the role of each sensory pathway, segregated from the others, is an open question.

In this work, we focus on a subsystem of a fish school consisting of two fish swimming in line against a flow inside a channel. Our goal is to identify causal interactions between the fish in the presence of multiple distinct modes of interaction. To achieve this goal, we design a robotic platform with an actuated airfoil and a compliant flag that simulates two fish swimming in line against a flow. As shown in Figure 1b, the pitching motion of the upstream airfoil sheds vortices in the flow that interact with the downstream flag, which flaps in response to these flow disturbances. This represents a unidirectional hydrodynamic interaction similar to that observed in fish swimming in line (Porfiri *et al.* 2021; Thandiackal & Lauder, 2023). The use of the compliant flag downstream allows for a larger response to the vortices and a potentially stronger hydrodynamic coupling than that produced by an airfoil pitching downstream, as previously studied by others (Kurt & Moored, 2018; Rival *et al.* 2011; Zhang *et al.* 2018). An electromechanical coupling between the airfoil and the flag is used to incorporate an additional unidirectional interaction pathway from the upstream to the downstream body, portraying, for instance, the effect of visual interaction. The potential of robotic set-ups for the study of hydrodynamic interactions in fish schools has been demonstrated in several studies (Ko *et al.* 2023; Lauder *et al.* 2011; Li *et al.* 2020; Marras and Porfiri, 2012; Thandiackal & Lauder, 2023; Zhang *et al.* 2019). Overall, our experimental set-up creates a controlled environment that incorporates distinct interaction pathways between two fish-like bodies positioned in line.

In order to study the influence of the upstream body on the downstream one, we employ the information-theoretic measure of transfer entropy (Schreiber, 2000). Transfer entropy is a measure of asymmetry in the interaction of two coupled stochastic processes (Bossomaier *et al.* 2016). It is emerging as the statistical approach of choice for studying pairwise interactions in complex systems in such wide-ranging fields as climate science, collective behaviour, neuroscience and finance (Staniek & Lehnertz, 2008; Butail *et al*. 2016; Stetter *et al.* 2012; Vicente *et al.* 2011; Shaffer & Abaid, 2020; Camacho *et al.* 2021; Campuzano *et al.* 2018; Hlinka *et al.* 2013; Valentini *et al.* 2021; Sandoval Jr, 2014). Previous work by Zhang *et al.* (2018) investigated the use of transfer entropy to elucidate the causal relationships between two tandem pitching airfoils communicating through the flow. The study involved interaction only via the hydrodynamic pathway and the response of the rigid airfoil downstream was limited. To address these limitations and to disentangle multiple sensory pathways, in this work: (i) we study the influence of a pitching airfoil on a compliant flag with multiple coexisting pathways of interaction – hydrodynamic and electromechanical, and (ii) we further conduct flow measurements to acquire information regarding the hydrodynamic pathway. We combine transfer entropy with experimental diagnostics/measurements to segregate the individual pathways of interaction from the airfoil to the flag. We do so by conditioning transfer entropy on the flow-related information/measurement. This conditional transfer entropy is demonstrated to reduce the overall interaction between the airfoil and the flag and predict the appropriate time delays of the interaction pathways.

The remainder of the paper is organised as follows. In § 2, the experimental set-up is described in detail, followed by a discussion of the three specific experimental conditions examined in this work. This

https://doi.org/10.1017/flo.2025.14 Published online by Cambridge University Press

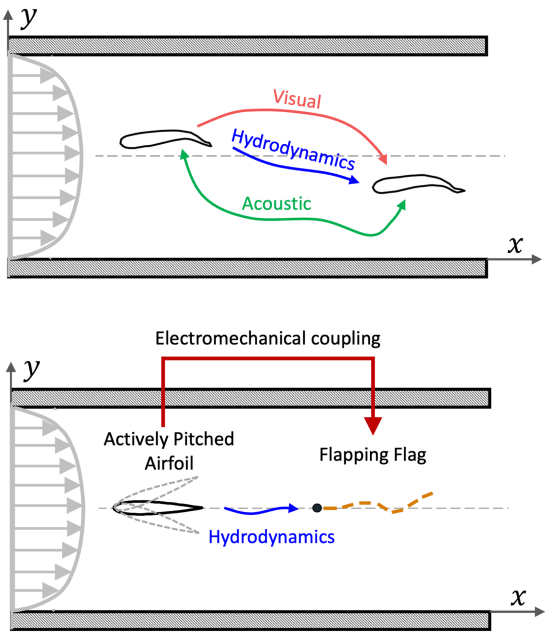

Figure 1. *Schematic representation of the proposed experimental approach. Top figure shows two fish swimming in a water channel and interacting via three distinct sensory pathways – visual, hydrodynamic and acoustic. Bottom figure shows a mechanical set-up that simulates the two fish swimming steadily against a channel flow, constituted by an actively pitching airfoil upstream and a compliant flag downstream. The airfoil influences the flag via two separate interaction pathways – hydrodynamics and electromechanical.*

section further details the experimental measurements and movement tracking involved together with the proposed statistical measures for detecting interactions along different pathways by analysing the experimental data. § 3 first demonstrates the processing of the recorded time series from experiments to prepare them for the transfer entropy analysis. Following this, the results and analyses of each of the three experimental cases are described. Finally, the main conclusions drawn from this study are outlined in § 4.

2. Methods

2.1. Experimental design

Experiments were conducted in an open water channel from Engineering Laboratory Design, Inc. The test section, shown in Figure 2(a), is $29\,\mathrm{cm}$ long with a rectangular cross-section of dimension $10\,\mathrm{cm} \times 15\,\mathrm{cm}$. The incoming flow was conditioned (straightening and reducing turbulence intensity) by passing it through a honeycomb section. An extruded airfoil was positioned towards the upstream end of the test section and a compliant flag was positioned in line with the airfoil and $10.4\,\mathrm{cm}$ downstream from its leading edge.

The airfoil was 3D-printed with a NACA 0012 cross-sectional geometry. It had a chord length of $c = 5\,\mathrm{cm}$, spanwise length of $6.9\,\mathrm{cm}$ and was designed to undergo a pitching motion about a pivot shaft located at 20% of the airfoil chord while remaining stationary otherwise. The airfoil's pitching motion was actively regulated by a servo-motor controlled by an Arduino Uno microcontroller board, programmed with the Arduino $1.8.19$ software package. The airfoil was subjected to continuous low-amplitude periodic pitching interspersed with sudden random startling motions of higher amplitude.

https://doi.org/10.1017/flo.2025.14 Published online by Cambridge University Press

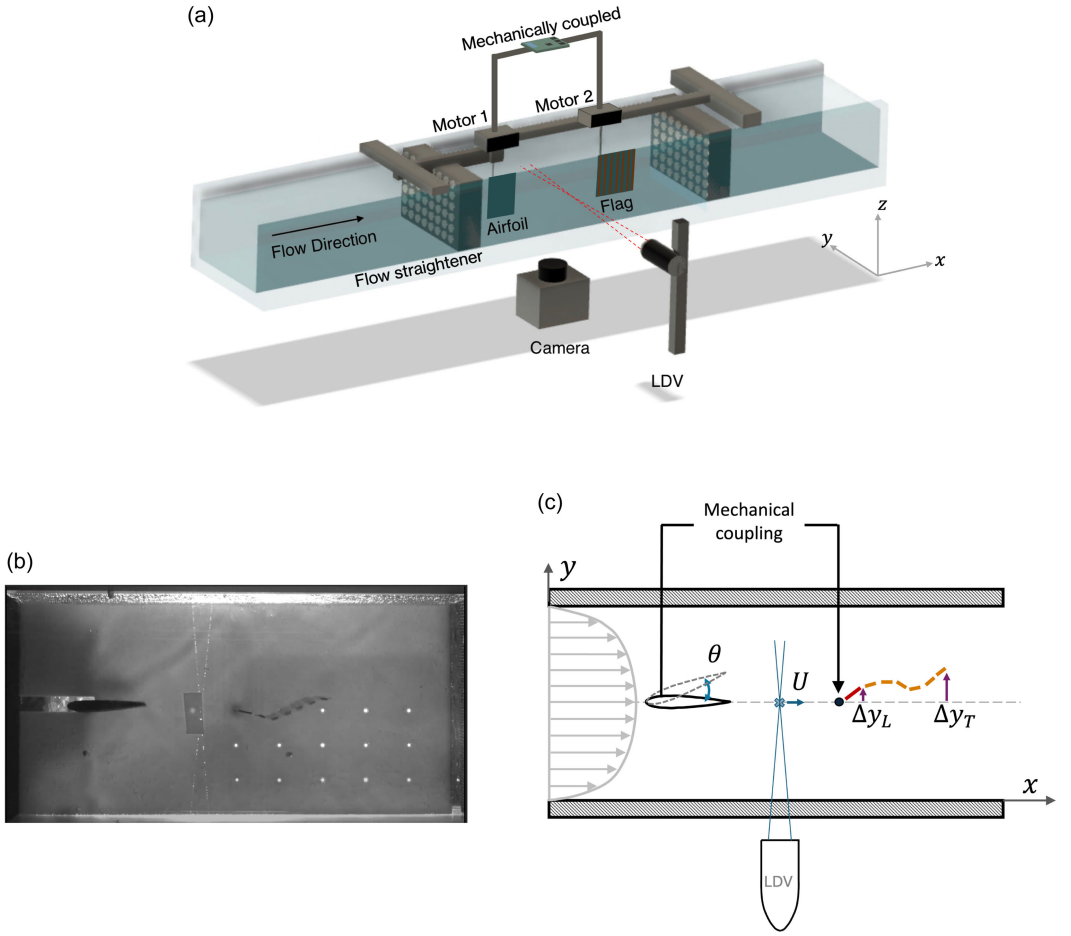

Figure 2. *Experimental set-up in a water channel: (a) three-dimensional view of the test section with an upstream airfoil and a downstream flag, a camera recording the bottom view of the test section, and laser Doppler velocimetry system measuring the streamwise flow velocity between the airfoil and the flag; (b) two-dimensional view of the test section from the bottom of the water channel as captured by the camera; and (c) a schematic representation of the two-dimensional test section with the tracked variables marked.*

A flag with dimensions of $6.98\,\mathrm{cm}$ length $\times 6.9\,\mathrm{cm}$ height was constructed. The design included: a $1\,\mathrm{mm}$ diameter $69\,\mathrm{mm}$ long flag pole; a Mylar sheet that covered the entire flag area; two $7\,\mathrm{mm} \times 69\,\mathrm{mm}$ copper strips anchored to the pole and to the two sides of the Mylar sheet forming the first fixed rib (leading rib); and six pairs of $4\,\mathrm{mm} \times 69\,\mathrm{mm}$ copper strips firmly fastened to either side of the Mylar sheet forming the remaining six ribs of the flag with $5.5\,\mathrm{mm}$ gaps between two ribs. The flag's design, particularly its mass density and bending stiffness, guaranteed flexibility and capacity to flap (Giacomello & Porfiri, 2011). It also prevented torsional motion of the flag along the streamwise and spanwise axes, effectively reducing its motion to two dimensions and led to flutter instability of the flag at very high flow speeds ($\geq 0.5\,\mathrm{m/s}$). The flag was securely positioned $5.4\,\mathrm{cm}$ downstream from the airfoil trailing edge. In the presence of a flow, a major portion of the flag downstream of the first anchored rib was free to flap passively in response to the fluctuating flow structures produced by the upstream airfoil's pitching. The first anchored rib of the flag was actuated to undergo periodic pitching motion, similar to the airfoil, using a second servo-motor controlled by the same microcontroller board.

https://doi.org/10.1017/flo.2025.14 Published online by Cambridge University Press

In all experiments, the airfoil's periodic pitching motion was maintained at a frequency of 3 Hz and amplitude of 15°. Additionally, we included a random startling motion of 40° angular deflection. The direction of the startle was chosen randomly and the time duration between two consecutive startles were sampled from a uniform random distribution in 5 ± 1.5 s. Experiments were conducted in the channel with static water (no flow) as well as with water flowing steadily through the channel. The inflow speed in the test section was maintained at $U_0 = 0.394$ m/s at the centreline (recorded using laser Doppler velocimetry described later in the section). This represents a chord-based Reynolds number of $Re = U_0 c/\nu = 21850$ and kinematic viscosity of water at room temperature is $\nu \approx 9 \times 10^{-7} \mathrm{m}^2/\mathrm{s}$.

2.2. Experimental cases

We performed experiments for the following conditions:

(i) Hydrodynamic interaction: to study the effect of hydrodynamic interaction between the airfoil and the flag, the flow channel was operated at a steady flow speed. The airfoil was subjected to periodic pitching motion superimposed with startling motions at random time intervals. The flag was not actuated and underwent flapping motion in response to the vortices generated by the upstream pitching airfoil.

(ii) Hydrodynamic + electromechanical interaction: to obtain hydrodynamic and electromechanical interaction between the airfoil and the flag, we maintained a steady flow of water in the channel and periodic pitching along with random startles in the airfoil. In addition, the first rib of the flag was electromechanically coupled to the airfoil motion. This was done by imposing the airfoil's pitching and startling motion on the flag's leading rib at a specific time delay ($\Delta_{AF} = 0.1\,\mathrm{s}, 0.3\,\mathrm{s}$) along with a certain degree of random noise. The noise was introduced in the form of additional 'noise startles' with a mean time gap of $\Delta_{no} = 0.04\mathrm{s}, 0.08\mathrm{s}$.

(iii) Electromechanical interaction: to study the case of only electromechanical interaction between the airfoil and the flag, experiments were conducted in static water. A periodic pitching motion interspersed with random startles was imposed on the airfoil and also on the flag with a time lag and added noise, similar to the previous case.

2.3. Measurement and tracking

Two forms of measurement were conducted during the experiments:

(i) Camera recording: a high-resolution camera (Point Grey Flea 3 USB camera; Point Grey, Richmond, Canada) was utilised to capture a two-dimensional view of the full test section ($29\,\mathrm{cm} \times 15\,\mathrm{cm}$), including the movement of the airfoil and the flag, as observed from below the water channel (Figure 2b). To document these sequences, the open-source software package, OBS Studio, was employed. The experimental footage was recorded at a resolution of 1920×1080 pixels and at a rate of 60 frames/s. Before experimental trials, the camera was calibrated by capturing and processing a video with a length-scale marked ruler in the test section. Correcting for any scale or distortion in the camera recordings, the calibration process enabled precise measurement of all movements within the test section.

(ii) Laser Doppler velocimetry: high spatial and temporal resolution fluid flow velocity measurements were made using the non-invasive laser Doppler velocimetry (LDV) technique (Foreman *et al.* 1965; Kalkert & Kayser, 2006). An optical technique that measures the velocity of passive tracer particles in a flow by analyzing the frequency shift of the laser light scattered by the moving particles. A single-component LDV system (Dantec Dynamics, Skovlunde, Hovedstaden, Denmark) was used to measure the instantaneous streamwise component of the flow velocity, U,

https://doi.org/10.1017/flo.2025.14 Published online by Cambridge University Press

at the channel centreline 3 cm downstream from the trailing edge of the airfoil. The BSA Flow software was used to record the LDV measurement over the course of each experiment. As LDV is dependent on light scattered by particles passing through the measurement volume, the measurement of U was not uniformly spaced in time. Polyamide particles were added to the flow to increase the sampling rate.

During each experiment, videos of the test section view and LDV measurement of flow velocity were recorded for a duration of 180 s. The recorded videos were processed to track the movements of the airfoil and flag by a program developed in MATLAB R2021b, using utilities available in its image processing toolbox. Specifically, the following quantities were tracked: the pitching angle of the airfoil, $\theta(t)$, the spanwise deflection of the leading rib of the flag, $\Delta y_L(t)$, and the spanwise deflection of the trailing rib of the flag, $\Delta y_T(t)$, as marked in Figure 2c.

2.4. Information-theoretic measures

Information theory is rooted in the concept of Shannon entropy (Shannon, 1948) that encodes the uncertainty or information content of a random variable X

$$H(X) = -\sum_{x\in\chi} p(x)\log p(x), \tag{2.1}$$

where $p(x)$ is the probability of an outcome x in the set of all possible outcomes (χ) of X; we use base 2 for the logarithms throughout the manuscript so that entropy is measured in bits. Similarly, the joint entropy of two random variables X and Y is given by

$$H(X,Y) = -\sum_{x\in\chi, y\in\gamma} p(x,y)\log p(x,y), \tag{2.2}$$

where γ is the set of all possible outcomes of Y. The conditional entropy of X given Y is

$$H(X|Y) = -\sum_{x\in\chi, y\in\gamma} p(x,y)\log p(x|y). \tag{2.3}$$

For two discrete-time stationary random processes, $X = \{X_n\}_{n=1}^{\infty}$ and $Y = \{Y_n\}_{n=1}^{\infty}$, where n is the time index, the influence (Wiener, 1956) of X on Y can be discerned by utilising transfer entropy (Schreiber, 2000; Wibral *et al.* 2013), defined as follows:

$$\begin{aligned}\mathrm{TE}_{X\to Y}(\delta) &= H\left(Y_n|Y_{n-1}\right) - H\left(Y_n|Y_{n-1}, X_{n-\delta}\right)\\ &= \sum_{\substack{y_n, y_{n-1},\\ x_{n-\delta}}} p\left(y_n, y_{n-1}, x_{n-\delta}\right)\log\left[\frac{p\left(y_n|y_{n-1}, x_{n-\delta}\right)}{p\left(y_n|y_{n-1}\right)}\right].\end{aligned} \tag{2.4}$$

Transfer entropy from X to Y is the reduction in uncertainty of target Y_n given its recent past, Y_{n-1}, due to the knowledge of the source's past state, $X_{n-\delta}$. Therefore, $\mathrm{TE}_{X\to Y}$ captures the influence of X on Y with a time lag of δ time steps. Likewise, $\mathrm{TE}_{Y\to X}$ quantifies the influence of Y on X. When X and Y have an asymmetric causal interaction, net transfer entropy, $\mathrm{net\,TE}_{X\to Y} = \mathrm{TE}_{X\to Y} - \mathrm{TE}_{Y\to X}$, can be used to indicate the predominant direction of influence.

If an additional random process Z_n is related to the X-Y dynamics, we quantify the causal dependence through

$$\begin{aligned}&\mathrm{TE}_{X\to Y|Z}(\delta_1,\delta_2) = H\left(Y_n|Y_{n-1}, Z_{n-\delta_2}\right) - H\left(Y_n|Y_{n-1}, X_{n-\delta_1}, Z_{n-\delta_2}\right)\\ &= \sum_{\substack{y_n, y_{n-1},\\ x_{n-\delta_1}, z_{n-\delta_2}}} p\left(y_n, y_{n-1}, x_{n-\delta_1}, z_{n-\delta_2}\right)\log\left[\frac{p\left(y_n|y_{n-1}, x_{n-\delta_1}, z_{n-\delta_2}\right)}{p\left(y_n|y_{n-1}, z_{n-\delta_2}\right)}\right],\end{aligned} \tag{2.5}$$

which is referred to as conditional transfer entropy (Sun & Bollt, 2014). Conditional transfer entropy from X to Y conditioned on Z represents the influence of the past of X (delay of δ_1 steps) on current Y, accounting for the knowledge of its own immediate past as well as the past of Z at a delay of δ_2 steps.

https://doi.org/10.1017/flo.2025.14 Published online by Cambridge University Press

Accurate estimation of these measures requires computation of up to a four-dimensional joint probability mass function (PMF), which can be challenging to estimate with a finite number of data samples. To circumvent this issue, we symbolised each time series using a dynamics-based approach (Porfiri & Marín, 2017) with an embedding dimension of $m = 2$. This approach converts a time series (X_n) to symbolised time series $(\pi_{X\,n})$ of 1 and 0 based on whether the value is increasing or decreasing, respectively, at a given time instant. The estimated PMF of the symbolised time series is accurate and robust to noise since the finite dataset is split between only two bins. Once the joint PMFs are estimated, transfer entropy and conditional transfer entropy are obtained using equations (2.4) and (2.5).

Once the transfer entropy is estimated from experimental data, it is pertinent to conduct statistical testing in order to infer whether the suggested causal influence is statistically significant. For transfer entropy, $\mathrm{TE}_{X\to Y}$, we generated a surrogate distribution of the transfer entropy by following a random permutation test. We randomly shuffled the source time series $\{X_n\}$, keeping the target time series unchanged, to maintain the link between it $\{Y_n\}$ and its past $\{Y_{n-1}\}$. We computed the corresponding transfer entropy to generate $N_{\mathrm{sur}} = 10000$ samples for the surrogate distribution. To test if conditioning on Z significantly reduces transfer entropy, $\mathrm{TE}_{X\to Y|Z}$, we generated a surrogate distribution by shuffling the Z time series $N_{\mathrm{sur}} = 10000$ times, while maintaining the link between the source and target (X-Y). The transfer entropy (or conditional transfer entropy) value was considered to be significant if the value was in the right (or left) tail of the surrogate distribution with a p-value smaller than 0.05. This enabled us to assess: (i) whether transfer entropy from a source to a target is significantly greater than that between a random source to the same target, and (ii) whether conditioning transfer entropy on a relevant variable Z reduced the transfer entropy as compared with conditioning on a random unrelated time series.

3. Results

In this section, we analyse the experimental observations using transfer entropy-based methods. First, the recorded time series of movements and flow velocity are illustrated, followed by a discussion on the processing of the time series prior to conducting information-theoretic analysis. Then, results of the three experimental conditions of interaction between the airfoil and the flag outlined in § 2.2 are discussed individually.

3.1. Pre-processing of time series

The experimental measurement and tracking (§ 2.3) yields raw time-series data of the airfoil pitching angle θ, flag leading rib deflection Δy_L, flag trailing rib deflection Δy_T and LDV-recorded streamwise flow speed U, as shown in the left panel of Figure 3. The airfoil angle θ demonstrates the periodic pitching motion interspersed with high-magnitude startles appearing at random time instants. The flag (both Δy_L and Δy_T) responds to the unsteady flow vortices generated by the pitching airfoil and demonstrates similar periodic and startling motions as the airfoil, only with a discernible time delay. The instantaneous streamwise flow speed U, on the other hand, does not exhibit a periodic behaviour and appears to be relatively more noisy, characteristic of a turbulent flow. Towards preparing the time series for the calculation of the information-theoretic measures, we sought to temporally match all the time series, suppress the effects of measurement noise, and address superfluous periodicity. These goals were pursued through the following steps.

Seasonal adjustment: the first three time series, $\theta, \Delta y_L$ and Δy_T, were recorded at uniformly spaced frequency of 60 Hz with a distinct seasonality in their behaviour. The periodic pitching helps maintain a continuous interaction between the airfoil and the flag, but it is the random startles and other mechanical noise that sustain the stochastic nature of the time series and is essential in applying statistical methods for causal inference. Therefore, prior to conducting the information-theoretic analysis, the time series must be seasonally adjusted, as commonly done in econometrics (Porfiri *et al.* 2019). We performed a seasonal adjustment on the θ, Δy_L and Δy_T time series, employing the multiple seasonal-trend

https://doi.org/10.1017/flo.2025.14 Published online by Cambridge University Press

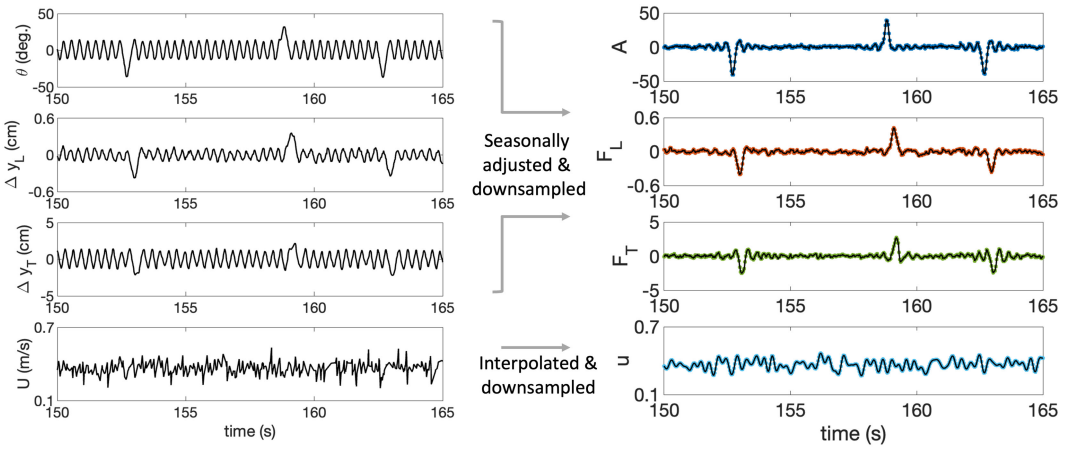

Figure 3. *Portion of the raw time series (left) and corresponding processed time series (right) of (from top to bottom): airfoil pitching angle (raw: θ and processed: A), flag's leading rib deflection (Δy_L and F_L), flag's trailing rib deflection (Δy_T and F_T) and streamwise flow speed recorded by LDV (U and u). The coloured dots in the plots on the right represent the downsampled time series used for symbolisation and later for transfer entropy analysis.*

decomposition using LOESS (locally estimated scatterplot smoothing) package in Python 3.9.7 to eliminate the "seasonal" trends in the data. This results in the processed time series of A for the airfoil's motion, F_L for the flag's leading rib motion and F_T for the flag's trailing rib motion as depicted in the right column of Figure 3. Disregarding the oscillations, these time series primarily encapsulate the startling motions. To remove experimental noise linked to mechanical movements or measurements, the time series were downsampled from the recorded 60 frames per second to 30 data points per second.

Interpolation: unlike the image-tracked motion of the airfoil and the flag, U was measured whenever a particle was tracked crossing the LDV measurement volume and was therefore non-uniformly spaced in time (~ 15 data points per second on average). Thus, U was interpolated and resampled to obtain a time series u that aligned in time with the uniformly spaced downsampled time series of A, F_L and F_T.

Symbolisation: finally, these time series were symbolised with an embedding dimension of $m = 2$ (as explained in § 2.4) to yield π_A, π_{F_L}, π_{F_T} and π_u (Figure 4). The symbolised time series were assigned binary values of 0 and 1, depending on whether it decreased or increased in value from one time step to the next. This results in probability estimation that is more robust to noise. These symbolised time series at a constant time increment of $\Delta t = 1/30\text{s} \approx 0.033$ s were finally used for the information-theoretic analysis. Such a symbolic representation is often adapted in information-theoretic analysis (López *et al.* 2010; Ruiz-Marin *et al.* 2010) when the relative change in the time series is more important than the precise values they attain at each time instance.

3.2. Hydrodynamic interaction

First, we analyse the experimental case of an actively controlled airfoil and passive flag in a steady flow inside the water channel. In this case, the leading rib of the flag remains fixed parallel to the streamwise axis and the airfoil and the flag interact primarily via the flow (hydrodynamic pathway). We compute transfer entropy from the airfoil to the flag's trailing rib and *vice versa* using Equation (2.4) and illustrate its variation with the time delay (δ) between the airfoil and the flag in Figure 5a. We observe that $\mathrm{TE}_{A\to F_T}$ is typically higher than $\mathrm{TE}_{F_T\to A}$ at nearly all time lags, suggesting a positive $\mathrm{net\ TE}_{A\to F_T}$. This implies that the airfoil has a stronger influence on the flag than the flag has on the airfoil, due to the fact that the compliant flag responds to the vortices shed by the pitching motion of the airfoil. The figure further shows that $\mathrm{TE}_{A\to F_T}$ attains a maximum at a time delay of $\delta_0 = 10\Delta t \approx 0.33$ s, consistent with

https://doi.org/10.1017/flo.2025.14 Published online by Cambridge University Press

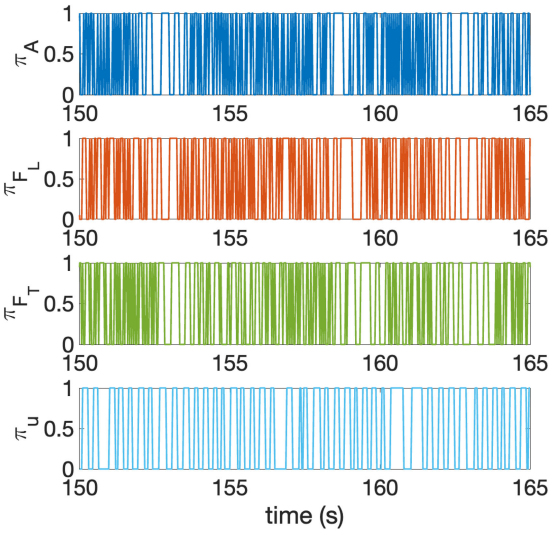

Figure 4. *Portion of the symbolised time series of the airfoil pitching angle (raw: π_A), flag's leading rib deflection (π_{F_L}), flag's trailing rib deflection (π_{F_T}) and streamwise flow speed recorded by LDV (π_u), directly used for the transfer entropy analysis.*

our estimated time taken by the flow (based on the maximum streamwise speed U_0 at the centreline) to reach the flag's trailing rib from the airfoil's trailing edge of ~ 0.3 s.

To test the statistical significance of $\mathrm{TE}_{A\to F_T}(\delta_0)$ against chance, we compare with its surrogate distribution created by randomly shuffling the source time series (π_A) $N_{\mathrm{sur}} = 10\,000$ times while preserving the dynamics of the target (π_{F_T}), as described in § 2.4. The surrogate probability distribution is illustrated in Figure 5b along with the peak value of $\mathrm{TE}_{A\to F_T}$. It is evident that $\mathrm{TE}_{A\to F_T}(\delta_0)$ is higher than chance ($p < 0.0001$), suggesting that there exists a causal relationship from the actively actuated upstream airfoil to the passively flapping downstream flag with a time delay of ~ 0.33 s.

Since the airfoil interacts with the flag through the flow, we condition the transfer entropy on the instantaneous flow-speed information encoded in the symbolised time series π_u. The conditional transfer entropy from airfoil to flag's trailing rib, conditioned on flow speed at an intermediate point, $\mathrm{TE}_{A\to F_T|u}(\delta_0, \delta_2)$, is plotted as a function of the time delay (δ_2) between the flow speed and the flag's tip deflection in Figure 5c. The figure illustrates that transfer entropy can decrease or increase upon conditioning, depending on the time lag between u and F_T. The conditional transfer entropy is minimum at $\delta_2 = \delta_{20} = 6\Delta t = 0.2$ s, suggesting that u can help predict the behaviour of F_T, 0.2 s ahead of time, due to the existence of the hydrodynamic pathway of interaction. This delay is close to our estimated time lag of 0.23 s, between the location of LDV measurement (u) and the tip of the flag (F_T) based on the centreline flow speed and the distance along the centreline.

The significance of the conditional transfer entropy with respect to a surrogate distribution obtained by shuffling the symbolised time series π_u is tested in Figure 5d. As described in § 2.4, such a surrogate distribution of the time series breaks the link with u, keeping the A-F_T dynamics intact. The value of $\mathrm{TE}_{A\to F_T|u}(\delta_0, \delta_{20})$ is found to be significantly reduced ($p = 0.0001$), demonstrating that conditioning on the LDV-recorded flow information significantly reduces the transfer entropy from the upstream airfoil to the downstream flag. This finding suggests that fluid flow is a primary information pathway in the airfoil–flag interaction.

3.3. Hydrodynamic and electromechanical interactions

Second, we study the experimental case in which both airfoil and flag are actively controlled in the presence of a steady flow. The actuation of the flag's leading rib follows that of the airfoil with a time

https://doi.org/10.1017/flo.2025.14 Published online by Cambridge University Press

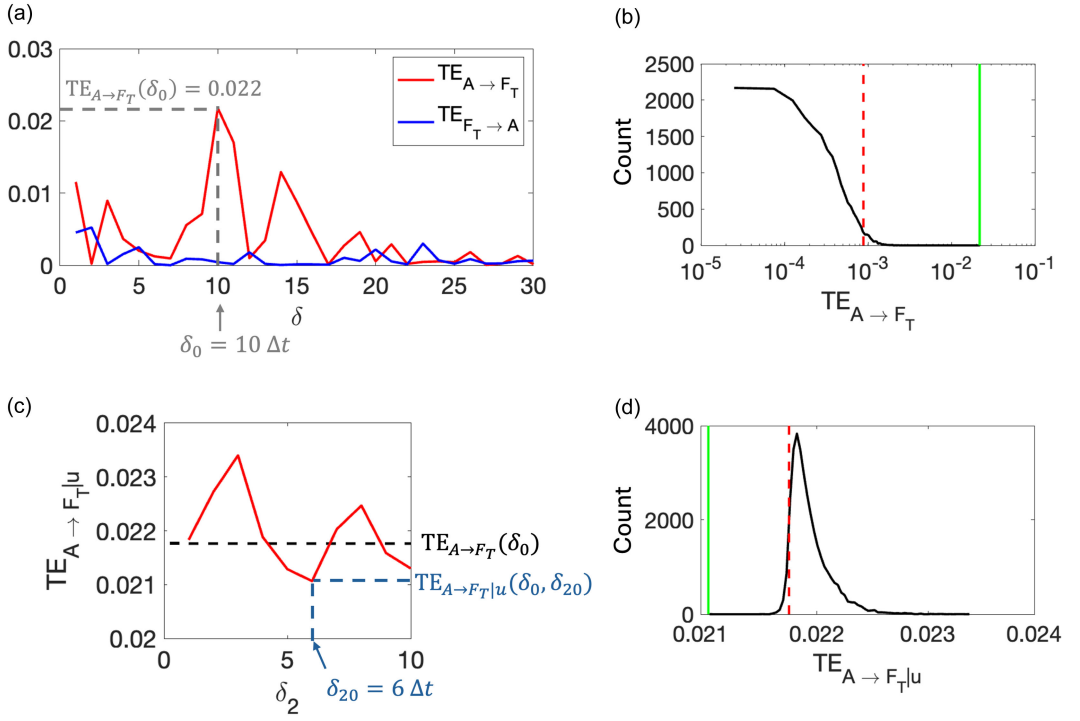

Figure 5. *Analysis of experiments with only hydrodynamic interaction: (a) transfer entropy from airfoil to trailing rib of the flag ($\mathrm{TE}_{A\to F_T}$) and from flag to airfoil ($\mathrm{TE}_{F_T\to A}$) for different delays δ between A and F_T. Peak $\mathrm{TE}_{A\to F_T}$ is observed at a delay of $\delta_0 = 10\Delta t$. At delay δ_0, (c) conditional transfer entropy from airfoil to flag conditioned on streamwise flow speed, $\mathrm{TE}_{A\to F_T|u}(\delta_0, \delta_2)$, as a function of time-delay (δ_2) between u and F_T. Minimum $\mathrm{TE}_{A\to F_T|u}$ is observed at delay $\delta_{20} = 6\Delta t$. Statistical tests: (b) $\mathrm{TE}_{A\to F_T}(\delta_0)$ with respect to its surrogate distribution and (d) $\mathrm{TE}_{A\to F_T|u}(\delta_0, \delta_{20})$ with respect to its surrogate distribution. In (b) and (d), green solid lines represent $\mathrm{TE}_{A\to F_T}(\delta_0)$ and $\mathrm{TE}_{A\to F_T|u}(\delta_0, \delta_{20})$, black solid lines represent their surrogate distributions and red dashed lines mark the 95 (or 5) percentile cutoff of the surrogate distributions.*

delay and added random noise. In this scenario, there are two major pathways of interaction between the airfoil and the flag – hydrodynamic and electromechanical. Figure 6a shows the variation of transfer entropies, $\mathrm{TE}_{A\to F_T}$ and $\mathrm{TE}_{F_T\to A}$, with the time delay between the airfoil and the flag's trailing rib (δ). Similar to the previous case, $\mathrm{TE}_{A\to F_T} > \mathrm{TE}_{F_T\to A}$ for most δ values, suggesting a stronger influence of the airfoil on the flag than *vice versa*. The peak $\mathrm{TE}_{A\to F_T}$ occurs at $\delta_0 = 11\Delta t = 0.37$ s, which is greater than the time delay of interaction identified in the presence of the hydrodynamic pathway alone in the previous case ($\delta_0 = 0.3$ s). This indicates that the combined presence of the electromechanical interaction in addition to the hydrodynamic interaction increases the effective time lag of the causal influence of the airfoil's motion on the flag's tip to 0.37 s. Such a finding is reasonable since the flag's leading rib is actuated with a delay of 0.3 s with respect to the airfoil and the transmission of the deflection from the leading rib of the flag to its trailing rib takes additional time. Therefore, the overall time delay in this experimental case is expected to be greater than the previous one. Further, the peak transfer entropy $\mathrm{TE}_{A\to F_T}(\delta_0)$ is statistically significant (Figure 6b), illustrating that in this experimental case as well, the airfoil has an overall causal influence on the flag.

In this experimental condition, the airfoil interacts with the flag via two distinct pathways – hydrodynamic and electromechanical. The LDV-measured speed *u* encodes part of the flow information while the deflection of the flag's leading rib F_L encodes the electromechanical information. First, we

https://doi.org/10.1017/flo.2025.14 Published online by Cambridge University Press

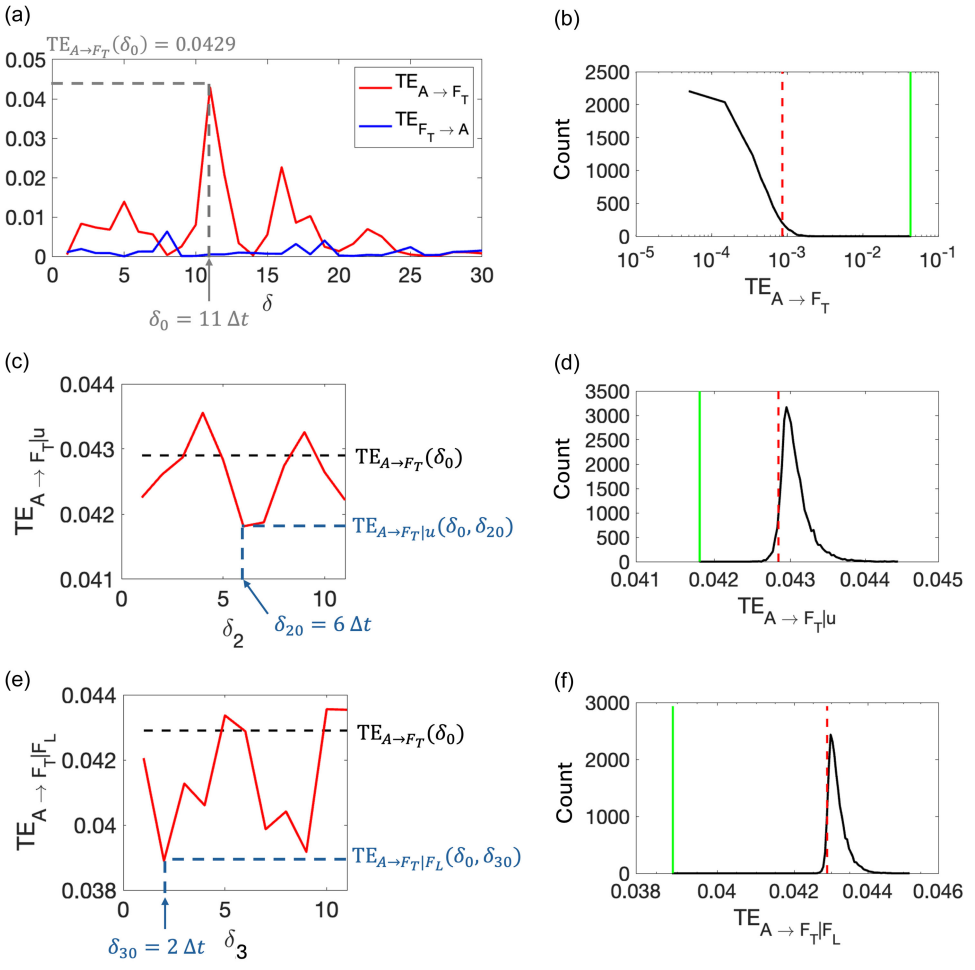

Figure 6. *Analysis of experiments with hydrodynamic and electromechanical interaction: (a) transfer entropy from airfoil to trailing rib of the flag ($\mathrm{TE}_{A\to F_T}$) and from flag to airfoil ($\mathrm{TE}_{F_T\to A}$) for different delays δ between A and F_T. Peak $\mathrm{TE}_{A\to F_T}$ is observed at a delay of $\delta_0 = 11\Delta t$. At delay δ_0, (c) conditional transfer entropy from airfoil to flag conditioned on streamwise flow speed, $\mathrm{TE}_{A\to F_T|u}(\delta_0,\delta_2)$, as a function of time delay δ_2 between u and F_T (minimum $\mathrm{TE}_{A\to F_T|u}$ is observed at delay $\delta_{20} = 6\Delta t$) and (e) conditional transfer entropy from airfoil to flag conditioned on flag's leading rib deflection ($\mathrm{TE}_{A\to F_T|F_L}(\delta_0,\delta_3)$) as a function of time delay δ_3 between F_L and F_T (minimum $\mathrm{TE}_{A\to F_T|F_L}$ is observed at delay $\delta_{20} = 2\Delta t$). Statistical tests: (b) $\mathrm{TE}_{A\to F_T}(\delta_0)$ with respect to its surrogate distribution, (d) $\mathrm{TE}_{A\to F_T|u}(\delta_0,\delta_{20})$ with respect to its surrogate distribution and (f) $\mathrm{TE}_{A\to F_T|F_L}(\delta_0,\delta_{30})$ with respect to its surrogate distribution. In (b), (d) and (f), green solid lines represent $\mathrm{TE}_{A\to F_T}(\delta_0)$, $\mathrm{TE}_{A\to F_T|u}(\delta_0,\delta_{20})$ and $\mathrm{TE}_{A\to F_T|F_L}(\delta_0,\delta_{30})$, black solid lines represent their surrogate distributions and red dashed lines mark the 95 (or 5) percentile cutoff of the surrogate distributions.*

study the conditional transfer entropy conditioned on u, $\mathrm{TE}_{A\to F_T|u}$, at a fixed F_T-A time delay ($\delta = \delta_0$) and for different time lags (δ_2) between F_T and u, as illustrated in Figure 6c. It is evident that conditioning on u is most effective in reducing the transfer entropy at a time delay of $\delta_{20} = 6\Delta t = 0.2$ s. This is identical to the time delay observed by transfer entropy analysis in the absence of the mechanical coupling, which one would expect since the hydrodynamic coupling is independent of the electromechanical coupling. Compared with the surrogate distribution with shuffled u time series in Figure 6d, the conditional transfer entropy $\mathrm{TE}_{A\to F_T|u}(\delta_0,\delta_{20})$ value is significantly less ($p = 0.0001$). Even in the presence

https://doi.org/10.1017/flo.2025.14 Published online by Cambridge University Press

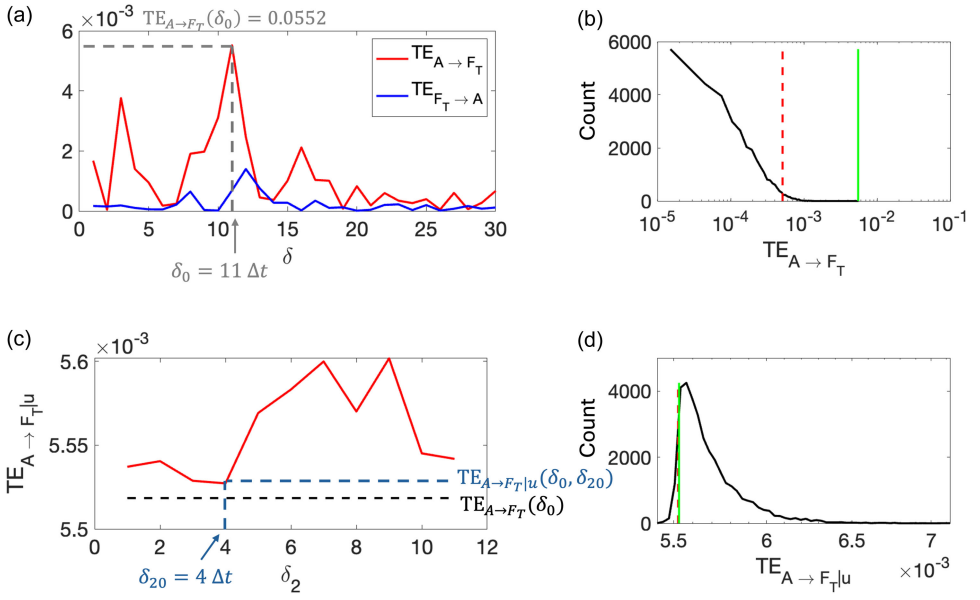

Figure 7. *Analysis of experiments with only electromechanical interaction: (a) transfer entropy from airfoil to trailing rib of the flag (*$\mathrm{TE}_{A\to F_T}$*) and from flag to airfoil (*$\mathrm{TE}_{F_T\to A}$*) for different delays* δ *between A and* F_T*. Peak* $\mathrm{TE}_{A\to F_T}$ *is observed at a delay of* $\delta_0 = 11\Delta t$*. At delay* δ_0*, (c) conditional transfer entropy from airfoil to flag conditioned on streamwise flow speed,* $\mathrm{TE}_{A\to F_T|u}(\delta_0, \delta_2)$*, as a function of timedelay (* δ_2*) between u and* F_T*. Minimum* $\mathrm{TE}_{A\to F_T|u}$ *is observed at delay* $\delta_{20} = 4\Delta t$*. Statistical tests: (b)* $\mathrm{TE}_{A\to F_T}(\delta_0)$ *with respect to its surrogate distribution and (d)* $\mathrm{TE}_{A\to F_T|u}(\delta_0, \delta_{20})$ *with respect to its surrogate distribution. In (b) and (d), green solid lines represent* $\mathrm{TE}_{A\to F_T}(\delta_0)$ *and* $\mathrm{TE}_{A\to F_T|u}(\delta_0, \delta_{20})$*, black solid lines represent their surrogate distributions and red dashed lines mark the* 95 *(or* 5*) percentile cutoff of the surrogate distributions.*

of other pathways of interaction, conditioning on the flow-speed information successfully reduces the transfer entropy from airfoil to flag, compared with conditioning it on a randomly shuffled time series. This suggests that the causal influence of airfoil on flag significantly reduces with the knowledge of the flow speed.

Next, we analyse conditional transfer entropy conditioned on F_L, $\mathrm{TE}_{A\to F_T|F_L}$, at a fixed F_T-A time delay ($\delta = \delta_0$) and for different time delays (δ_3) between F_T and F_L, in Figure 6e. The F_L-conditioning reduces transfer entropy from the airfoil to the flag's tip the most at a time lag of $\delta_{30} = 2\Delta t = 0.07$ s. This indicates that the time required for the deflection at the leading rib of the flag to propagate to its trailing rib is ≈ 0.07 s. The secondary minima at a time lag of $\delta_{30} = 9\Delta t = 0.3$ s indicates the presence of multi-time-scale information flow through the length of the slender flag from the leading rib to the trailing rib. Additionally, Figure 6f demonstrates that conditional transfer entropy is significantly less than the null distribution with a p-value of $p = 0.0001$. Therefore, conditioning on the mechanical coupling information significantly reduces the transfer entropy, as compared with conditioning the same on a randomly shuffled timeseries. This indicates that the overall causal influence of the airfoil on the flag significantly decreases on account of the knowledge of the motion of the flag's leading rib.

3.4. Electromechanical interaction

In the third case, the experiments were conducted in the absence of a flow, which implies that the airfoil and the flag primarily interact via electromechanical coupling only without any hydrodynamic interaction. As illustrated in Figures 7a and 7b, the transfer entropy analysis shows a significant influence

https://doi.org/10.1017/flo.2025.14 Published online by Cambridge University Press

of the airfoil's motion on the flag's tip deflection at a time delay of $\delta_0 = 11\Delta t = 0.37$ s. However, upon conditioning on u, conditional transfer entropy is greater than transfer entropy value for all time delays δ_2, as shown in Figure 7c. In addition, the minimum conditional transfer entropy, $\mathrm{TE}_{A\to F_T|u}(\delta_0, \delta_{20})$, is not significantly ($p = 0.07$) smaller than transfer entropy conditioned on a randomly shuffled time series (Figure 7d). We can infer that conditioning on flow information only reduces transfer entropy from airfoil to flag if a hydrodynamic interaction is present. Therefore, such a conditional transfer entropy can be used to test the presence or absence of hydrodynamic interaction pathway in an unknown case.

4. Discussion and conclusions

A controlled robotic set-up in a water channel was designed to recreate a simplified fish schooling subsystem. Experiments were conducted using an upstream pitching airfoil and a downstream flapping flag representing two fish swimming inline. The airfoil's motion influenced the flag's behaviour via two independent pathways – hydrodynamic and eletromechanical. The hydrodynamic coupling was constituted by vortex-induced pressure variations generated by the pitching of the upstream airfoil that causes the compliant flag downstream to flap in response. Further, the leading rib of the flag was actuated to follow the motion of the airfoil with a delay, therefore causing the flag to flap in response to the electromechanical coupling. Experiments were conducted under three conditions – (i) with only hydrodynamic coupling, (ii) with hydrodynamic and electromechanical coupling and (iii) with only electromechanical coupling. Besides monitoring the movements of both the airfoil and the flag, the LDV technique was employed to measure the streamwise flow speed at a midpoint. This data served as a source of information on the hydrodynamic interaction pathway between the airfoil and the flag.

The information-theoretic analysis was conducted using properly conditioned experimental data of the airfoil, flag and flow speed. It was demonstrated that transfer entropy from the airfoil to the flag can recognise and quantify the causal influence of the airfoil on the flag under all three experimental conditions. In addition, the method identifies the appropriate time delay of the interaction with reasonable accuracy. Our findings suggest that transfer entropy can be adapted to identify causal influence between units of a system that are interacting via single or multiple pathways.

By conditioning on a measurable physical quantity related to one pathway, that is, flow-speed information related to hydrodynamic coupling, one can reduce transfer entropy from the airfoil to the flag significantly. This conditional transfer entropy is competent in reducing the information flow from the airfoil to the flag on account of knowledge about the flow, if the hydrodynamic interaction exists. Similarly, conditioning on information related to the electromechanical coupling (undulation of the flag's leading rib) reduces the transfer entropy from the airfoil to the flag, only if the electromechanical coupling is present. This implies that conditional transfer entropy based on measured experimental data related to one particular interaction pathway helps disentangle the other pathways from this one.

The current study employs an experimental set-up with unidirectional interactions only, from the airfoil to the flag. In future work, transfer entropy based method will be formulated for similar systems to disentangle bidirectional interactions. While the present work demonstrates the ability of conditional transfer entropy in accounting for the contributions of different interaction pathways, it does not precisely quantify the contributions of each pathway of interaction. Overall, the study suggests that conditioning transfer entropy on experimentally measured relevant information, one can identify unknown interactions between different components of a fluid–structure interaction system and estimate the associated time lags of the processes of the system. In the future, this mechanism will be extended to distinguish the contributions of various interaction pathways within biological complex systems, such as fish schools. Our approach is expected to apply directly to spatially disperse schools where fish are far apart, so that one may hypothesise weak coupling between the units of the complex system (Porfiri & Marín, 2017, 2018). Prudence is warranted when dealing with dense schools for which the direct application of transfer entropy may lead to false inferences due to common driver and chain effects. Addressing these issues

https://doi.org/10.1017/flo.2025.14 Published online by Cambridge University Press

may require the use of causation entropy (Sun & Bollt, 2014; Sun *et al.* 2015) or the inclusion of coarse observables for the entire school (Wang *et al.* 2012).

Acknowledgements. The authors would like to thank Ms A. Ravindran for her help during the experimentation.

Data availability. Data and codes used in this work are available in a *Github repository*.

Funding. The research was supported by the National Science Foundation under Grant No. CMMI-1901697. R.D. would also like to acknowledge Indian Institute of Science for the Startup Research Grant.

Competing interests. The authors declare no conflict of interest.

Ethical standards. The research meets all ethical guidelines, including adherence to the legal requirements of the study country.

References

Arnold, G. P. (1969). The reactions of the plaice (Pleuronectes platessa L.) to water currents. *Journal of Experimental Biology*, *51*(3), 681–697.

Ashraf, I., Bradshaw, H., Ha, T.-T., Halloy, J., Godoy-Diana, R., & Thiria, B. (2017). Simple phalanx pattern leads to energy saving in cohesive fish schooling. *Proceedings of the National Academy of Sciences of the United States of America*, *114*(36), 9599–9604.

Bossomaier, T., Barnett, L., Harré, M., & Lizier, J. T. (2016). *An introduction to transfer entropy*. Springer.

Butail, S., Mwaffo, V., & Porfiri, M. (2016). Model-free information-theoretic approach to infer leadership in pairs of zebrafish. *Physical Review E*, *93*(4), 042411.

Camacho, M., Romeu, A., & Ruiz-Marin, M. (2021). Symbolic transfer entropy test for causality in longitudinal data. *Economic Modelling*, *94*, 649–661.

Campuzano, S. A., De Santis, A., Pavón-Carrasco, F. J., Osete, M. L., & Qamili, E. (2018). New perspectives in the study of the earth's magnetic field and climate connection: The use of transfer entropy. *PLoS One*, *13*(11), e0207270.

De Bie, J., Manes, C., & Kemp, P. S. (2020). Collective behaviour of fish in the presence and absence of flow. *Animal Behaviour*, *167*, 151–159.

Filella, A., Nadal, F., Sire, C., Kanso, E., & Eloy, C. (2018). Model of collective fish behavior with hydrodynamic interactions. *Physical Review Letters*, *120*(19), 198101.

Foreman, J. W., George, E. W., & Lewis, R. D. (1965). Measurement of localized flow velocities in gases with a laser doppler flowmeter. *Applied Physics Letters*, *7*(4), 77–78.

Giacomello, A., & Porfiri, M. (2011). Underwater energy harvesting from a heavy flag hosting ionic polymer metal composites. *Journal of Applied Physics*, *109*(8), 084903.

Hlinka, J., Hartman, D., Vejmelka, M., Runge, J., Marwan, N., Kurths, J., & Paluš, M. (2013). Reliability of inference of directed climate networks using conditional mutual information. *Entropy*, *15*(6), 2023–2045.

Hyacinthe, C., Attia, J., & Rétaux, S. (2019). Evolution of acoustic communication in blind cavefish. *Nature Communications*, *10*(1), 4231.

Kalkert, C., & Kayser, J. (2006). *Laser doppler velocimetry*. San Diego:PHYS173.

Kasumyan, A. O. (2004). The vestibular system and sense of equilibrium in fish. *Journal of Ichthyology*, *44*(2), S224.

Ko, H., Lauder, G., & Nagpal, R. (2023). The role of hydrodynamics in collective motions of fish schools and bioinspired underwater robots. *Journal of the Royal Society Interface*, *20*(207), 20230357.

Kurt, M., & Moored, K. W. (2018). Flow interactions of two-and three-dimensional networked bio-inspired control elements in an in-line arrangement. *Bioinspiration & Biomimetics*, *13*(4), 045002.

Ladich, F., & Winkler, H. (2017). Acoustic communication in terrestrial and aquatic vertebrates. *Journal of Experimental Biology*, *220*(13), 2306–2317.

Landeau, L., & Terborgh, J. (1986). Oddity and the 'confusion effect' in predation. *Animal Behaviour*, *34*(5), 1372–1380.

Larsson, M. (2012). Why do fish school? *Current Zoology*, *58*(1), 116–128.

Lauder, G. V., Lim, J., Shelton, R., Witt, C., Anderson, E., & Tangorra, J. L. (2011). Robotic models for studying undulatory locomotion in fishes. *Marine Technology Society Journal*, *45*(4), 41–55.

Li, L., Nagy, M., Graving, J. M., Bak-Coleman, J., Xie, G., & Couzin, I. D. (2020). Vortex phase matching as a strategy for schooling in robots and in fish. *Nature Communications*, *11*(1), 5408.

Liao, J. C., Beal, D. N., Lauder, G. V., & Triantafyllou, M. S. (2003). Fish exploiting vortices decrease muscle activity. *Science*, *302*(5650), 1566–1569.

Lombana, D. A. B., & Porfiri, M. (2022). Collective response of fish to combined manipulations of illumination and flow. *Behavioural Processes*, *203*, 104767.

https://doi.org/10.1017/flo.2025.14 Published online by Cambridge University Press

López, F., Matilla-García, M., Mur, J., & Marín, M. R. (2010). A non-parametric spatial independence test using symbolic entropy. *Regional Science and Urban Economics*, *40*(2–3), 106–115.
Major, P. F. (1978). Predator-prey interactions in two schooling fishes, Caranx ignobilis and Stolephorus purpureus. *Animal Behaviour*, *26*, 760–777.
Marras, S., Killen, S. S., Lindström, J., McKenzie, D. J., Steffensen, J. F., & Domenici, P. (2015). Fish swimming in schools save energy regardless of their spatial position. *Behavioral Ecology and Sociobiology*, *69*(2), 219–226.
Marras, S., & Porfiri, M. (2012). Fish and robots swimming together: Attraction towards the robot demands biomimetic locomotion. *Journal of the Royal Society Interface*, *9*(73), 1856–1868.
Pavlov, D. S., & Kasumyan, A. O. (2000). Patterns and mechanisms of schooling behavior in fish: A review. *Journal of Ichthyology*, *40*(2), S163.
Pitcher, T. J. (2001). Fish schooling. *Encyclopedia of ocean sciences: Marine biology*, pp. 337–349.
Pitcher, T. J., Magurran, A. E., & Winfield, I. J. (1982). Fish in larger shoals find food faster. *Behavioral Ecology and Sociobiology*, *10*(2), 149–151.
Porfiri, M., Karakaya, M., Sattanapalle, R. R., & Peterson, S. D. (2021). Emergence of in-line swimming patterns in zebrafish pairs. *Flow*, *1*, E7.
Porfiri, M., & Marín, M. R. (2017). Information flow in a model of policy diffusion: An analytical study. *IEEE Transactions on Network Science and Engineering*, *5*(1), 42–54.
Porfiri, M., & Marín, M. R. (2017). Symbolic dynamics of animal interaction. *Journal of Theoretical Biology*, *435*, 145–156.
Porfiri, M., & Marín, M. R. (2018). Inference of time-varying networks through transfer entropy, the case of a Boolean network model. *Chaos: An Interdisciplinary Journal of Nonlinear Science*, *28*, 103123.
Porfiri, M., Sattanapalle, R. R., Nakayama, S., Macinko, J., & Sipahi, R. (2019). Media coverage and firearm acquisition in the aftermath of a mass shooting. *Nature Human Behaviour*, *3*(9), 913–921.
Rival, D., Hass, G., & Tropea, C. (2011). Recovery of energy from leading-and trailing-edge vortices in tandem-airfoil configurations. *Journal of Aircraft*, *48*(1), 203–211.
Ruiz-Marin, M., Matilla-Garcia, M., García, J. A. C., González-Susillo, J. L., Romo-Astorga, A., González-Pérez, A., Ruiz, A., & Gayan, J. (2010). An entropy test for single-locus genetic association analysis. *BMC Genetics*, *11*(1), 1–15.
Saadat, M., Berlinger, F., Sheshmani, A., Nagpal, R., Lauder, G. V., & Haj-Hariri, H. (2021). Hydrodynamic advantages of in-line schooling. *Bioinspiration & Biomimetics*, *16*(4), 046002.
Sandoval, L.Jr (2014). Structure of a global network of financial companies based on transfer entropy. *Entropy*, *16*(8), 4443–4482.
Schreiber, T. (2000). Measuring information transfer. *Physical Review Letters*, *85*(2), 461–464.
Shaffer, I., & Abaid, N. (2020). Transfer entropy analysis of interactions between bats using position and echolocation data. *Entropy*, *22*(10), 1176.
Shannon, C. E. (1948). A mathematical theory of communication. *The Bell System Technical Journal*, *27*(3), 379–423.
Staniek, M., & Lehnertz, K. (2008). Symbolic transfer entropy. *Physical Review Letters*, *100*(15), 158101.
Stetter, O., Battaglia, D., Soriano, J., & Geisel, T. (2012). Model-free reconstruction of excitatory neuronal connectivity from calcium imaging signals. *PLoS Computational Biology*, *8*(8), 1–25.
Sun, J., & Bollt, E. M. (2014). Causation entropy identifies indirect influences, dominance of neighbors and anticipatory couplings. *Physica D: Nonlinear Phenomena*, *267*, 49–57.
Sun, J., Taylor, D., & Bollt, E. M. (2015). Causal network inference by optimal causation entropy. *SIAM Journal on Applied Dynamical Systems*, *14*(1), 73–106.
Thandiackal, R., & Lauder, G. (2023). In-line swimming dynamics revealed by fish interacting with a robotic mechanism. *eLife*, *12*, e81392.
Valentini, G., Pavlic, T. P., Walker, S. I., Pratt, S. C., Biro, D., & Sasaki, T. (2021). Naïve individuals promote collective exploration in homing pigeons. *eLife*, *10*, e68653.
Vicente, R., Wibral, M., Lindner, M., & Pipa, G. (2011). Transfer entropy—a model-free measure of effective connectivity for the neurosciences. *Journal of Computational Neuroscience*, *30*(1), 45–67.
Wang, X. R., Miller, J. M., Lizier, J. T., Prokopenko, M., Rossi, L. F., & de Polavieja, G. G. (2012). Quantifying and tracing information cascades in swarms. *PloS One*, *7*(7), e40084.
Weihs, D. (1973). Hydromechanics of fish schooling. *Nature*, *241*(5387), 290–291.
Wibral, M., Pampu, N., Priesemann, V., Siebenhühner, F., Seiwert, H., Lindner, M., Lizier, J. T., Vicente, R., & Hayasaka, S. (2013). Measuring information-transfer delays. *PLoS One*, *8*(2), e55809.
Wiener, N. (1956). The theory of prediction. *Modern mathematics for engineers: First series*. McGraw-Hill.
Zhang, P., Krasner, E., Peterson, S. D., & Porfiri, M. (2019). An information-theoretic study of fish swimming in the wake of a pitching airfoil. *Physica D: Nonlinear Phenomena*, *396*, 35–46.
Zhang, P., Rosen, M., Peterson, S. D., & Porfiri, M. (2018). An information-theoretic approach to study fluid–structure interactions. *Journal of Fluid Mechanics*, *848*, 968–986.

Cite this article: Das R, Peterson S D and Porfiri M (2025). Disentangling coexisting sensory pathways of interaction in schooling fish. *Flow*, *5*, E16. https://doi.org/10.1017/flo.2025.14